

AN ADAPTIVE DISCONTINUOUS GALERKIN MULTISCALE METHOD FOR ELLIPTIC PROBLEMS

DANIEL ELFVERSON[†], EMMANUIL H. GEORGOULIS[‡], AND AXEL MÅLQVIST[§]

Abstract. An adaptive discontinuous Galerkin multiscale method driven by an energy norm a posteriori error bound is proposed. The method is based on splitting the problem into a coarse and a fine scale. Localized fine scale constituent problems are solved on patches of the domain and are used to obtain a modified coarse scale equation. The coarse scale equation has considerably less degrees of freedom than the original problem. The a posteriori error estimate is used within an adaptive algorithm to tune the critical parameters, i.e., the refinement level and the size of the different patches on which the fine scale constituent problems are solved. The fine scale computations are completely parallelizable, since no communication between different processors is required for solving the constituent fine scale problems. The convergence of the method, the performance of the adaptive strategy and the computational effort involved are investigated through a series of numerical experiments.

Key words. multiscale, discontinuous Galerkin, a posteriori error estimate

AMS subject classifications. 65N30, 65N15

1. Introduction. Problems involving features on several different scales, usually termed multiscale problems, can be found in many branches of engineering science. Examples include the modelling of flow in porous media and through composite materials. Multiscale problems involving partial differential equations are often impossible to simulate with an acceptable accuracy when employing standard (single mesh) numerical methods. A different approach, usually coming under the general term of multiscale methods, consists of considering coarse and fine scale contributions to the solution, with the fine scale contributions approximated on localized patches. The fine scale contributions are then used to upscale a (modified) coarse scale problem to obtain an approximation to the global multiscale solution.

1.1. Previous work. Numerous multiscale methods have been developed during the last three decades, see, e.g., [8, 7] for some early works, or [17, 29, 16] and the references therein for exposition and recent developments. An important development is the Multiscale Finite Element Method by Hou and Wu [21], which was further developed in [13], with the introduction of oversampling to reduce resonance effects. Another approach is the, so-called, Variational Multiscale Method (VMS) of Hughes and co-workers [22, 23]. The idea in VMS is to decompose the problem into one coarse and one fine scale contribution. A modified coarse scale problem is then solved (using a finite element approach), so that the fine scale contribution is taken into account. To maintain the conformity of the resulting enriched finite element space homogeneous Dirichlet boundary conditions have been imposed on each fine-problem patch boundary. The Adaptive Variational Multiscale Method (AVMS) using the VMS framework, introduced by Larson and Målqvist [27], makes use of multiscale-type a posteriori error estimates to adapt automatically the coarse and

[†]Information Technology, Uppsala University, SE-751 05, Uppsala, Sweden. (daniel.elfverson@it.uu.se)

[‡]Department of Mathematics, University of Leicester, Leicester, UK. (emmanuil.georgoulis@le.ac.uk)

[§]Information Technology, Uppsala University, SE-751 05, Uppsala, Sweden. (axel.malqvist@it.uu.se)

fine scale meshsizes as well as the fine-problem patch-sizes. A a priori error analysis can be found in [30, 31].

An interesting alternative to conforming finite element methods is the class of discontinuous Galerkin (DG) methods, whereby the approximation spaces are element-wise discontinuous; the continuity of the underlying exact solutions of the problems are then imposed weakly. DG methods appeared in the 1970s and in the early 1980s [33, 28, 9, 5, 24] and have recently received renewed interest; we refer to the volumes [14, 15, 20, 34] and the references therein for a literature review. DG methods admit good conservation properties of the state variable and, due to the lack of inter-element continuity requirements are ideally suited for application to complex and/or irregular meshes. Also, there has been work to better cope with the case of high contrast diffusion; see e.g. [19] where a DG method based on weighted average is proposed and analysed.

Discontinuous Galerkin methods for solving multiscale problems have been discussed using the frameworks of the Multiscale Finite Element Method [1] and of the Heterogeneous Multiscale method [2]; see also [38, 37, 36, 35].

1.2. New contributions. In this work, we propose an *adaptive discontinuous Galerkin multiscale method* (ADG-MS) using the framework of VMS. The new DG method is based on weighted averages across the element interfaces. The adaptivity is driven by energy norm a posteriori error bounds. The method consists of solving localized problems on fine scale patches with homogeneous Neumann boundary conditions. Due to the lack of inter-element continuity requirements of the approximate solution in the DG framework, the Neumann-type fine scale problems, leading to non-conforming sub-grid corrections, are now admissible. These fine scale problems can be solved independently with localized right hand sides. In the a posteriori error estimate, the error is bounded in terms of the size of the different fine-scale patches and on both the fine-scale and the coarse-scale mesh sizes. An adaptive algorithm to tune all these parameters automatically is proposed. The numerical experiments show the good performance of the algorithm in a number of known benchmark problems.

1.3. Outline. The rest of this work is structured as follows. Section 2 is devoted to setting up the model problem, the basic DG discretization and some notation. A general framework for multiscale problems along with the discontinuous Galerkin multiscale method is derived in Section 3, with the multiscale a posteriori error estimator derived in Section 4. The implementation of the method and the adaptive algorithm are discussed in Section 5. Finally, in Section 6, a number of numerical experiments are presented, and some conclusions are drawn in Section 7.

2. Preliminaries.

2.1. Notation. Let $\omega \subseteq \mathbb{R}^d$, $d = 2, 3$ be an open polygonal domain. Denote the $L^2(\omega)$ -inner product by $(\cdot, \cdot)_{L^2(\omega)}$, and the corresponding norm by $\|\cdot\|_{L^2(\omega)}$. Also, let $H^1(\omega)$ be the Sobolev space with norm $\|\cdot\|_{H^1(\omega)} := (\|\cdot\|_{L^2(\omega)}^2 + \|\nabla \cdot\|_{L^2(\omega)}^2)^{1/2}$ and $H^s(\omega)$ the standard Hilbertian Sobolev space of index $s \in \mathbb{R}$. We shall also make use of the space $L^\infty(\omega)$ consisting of almost everywhere bounded functions, with norm $\|\cdot\|_{L^\infty(\omega)} := \text{ess sup}_\omega |\cdot|$; see, e.g., [3] for details. Finally, the d -dimensional Lebesgue measure will be denoted by $\mu_d(\cdot)$.

2.2. Model problem. Let $\Omega \subset \mathbb{R}^d$ be an open polygonal domain $\partial\Omega$, $d = 2, 3$, and consider the elliptic boundary value problem

$$-\nabla \cdot \alpha \nabla u = f \quad u \in \Omega, \quad (2.1)$$

$$n \cdot \alpha \nabla u = 0 \quad u \in \partial\Omega, \quad (2.2)$$

with $f \in L^2(\Omega)$ and $\alpha \in L^\infty(\Omega)$ such that $\alpha \geq \beta > 0$ almost everywhere, for some $\beta \in \mathbb{R}$. The solution $u \in H^1(\Omega)$ is unique up to a constant provided that $\int_\Omega f \, dx = 0$ is satisfied.

2.3. Discretization and subdivision. The domain Ω is subdivided into a locally quasi-uniform partition $\mathcal{K} = \{K\}$ satisfying the minimum angle condition [10] with the mesh function $h : \cup_{K \in \mathcal{K}} K \rightarrow \mathbb{R}$ defined element-wise by $h|_K := \text{diam}(K)$, $K \in \mathcal{K}$. Associated with the diffusion tensor, we consider the element-wise constant functions $\alpha^0, \alpha_0 : \cup_{K \in \mathcal{K}} K \rightarrow \mathbb{R}$ defined by the biggest and smallest eigenvalue of α , respectively, on each element K . We also define

$$\Gamma^B := \{e = \partial K \cap \partial\Omega, \forall K \in \mathcal{K} \text{ s.t. } \mu_{d-1}(\partial K \cap \partial\Omega) > 0\}, \quad (2.3)$$

$$\Gamma^I := \{e = \partial K_i \cap \partial K_j, \forall K_i, K_j \in \mathcal{K} \text{ s.t. } \mu_{d-1}(\partial K_i \cap \partial K_j) > 0 \text{ and } i \neq j\}, \quad (2.4)$$

i.e., Γ^B is the union of all boundary edges and Γ^I is the union of all interior edges (or faces when $d = 3$).

For $K_i, K_j \in \mathcal{K}$, with $\mu_{d-1}(\partial K_i \cap \partial K_j) > 0$, let K_i, K_j be denoted by K^+, K^- where K^+ is the element with the higher index. On interior element interfaces $e \in \Gamma^I$ we shall make use of the shorthand notation $v^+ := v|_{K^+}$, $v^- := v|_{K^-}$; on boundary edges we set $v^+ := v|_K$. We also define the weighted mean value by

$$\{v\}_w := w_{K^+(e)} v^+ + w_{K^-(e)} v^-, \quad (2.5)$$

where

$$w_{K^+(e)} := \frac{\alpha^0|_{K^-}}{\alpha^0|_{K^+} + \alpha^0|_{K^-}}, \quad w_{K^-(e)} := \frac{\alpha^0|_{K^+}}{\alpha^0|_{K^+} + \alpha^0|_{K^-}}, \quad (2.6)$$

for each $e \in \Gamma^I$ and

$$w_{K^+(e)} = 1, \quad w_{K^-(e)} = 0, \quad (2.7)$$

for $e \in \Gamma^B$. Further, the jump across element interfaces is defined by

$$[v] := v^+ - v^- \text{ for } e \in \Gamma^I, \quad \text{and} \quad [v] := v^+ \text{ for } e \in \Gamma^B, \quad (2.8)$$

and the harmonic mean value γ_e by

$$\gamma_e := \frac{2\alpha^0|_{K^+}\alpha^0|_{K^-}}{\alpha^0|_{K^+} + \alpha^0|_{K^-}}. \quad (2.9)$$

Also, n will denote the outward unit normal to ∂K^+ when $\mu_{d-1}(\partial K^+ \cap \partial K^-) > 0$; when $\mu_{d-1}(\partial K \cap \partial\Omega) > 0$, n will be the outward unit normal to $\partial\Omega$.

2.4. Discontinuous Galerkin method. For a nonnegative integer r , we denote by $\mathcal{P}_r(\hat{K})$, the set of all polynomials on \hat{K} of total degree at most r , if \hat{K} is the reference d -simplex or, of degree at most r in each variable, if \hat{K} the reference d -hypercube.

Consider the space $\mathcal{V} := \mathcal{V}_h + H^{1+\epsilon}(\Omega)$ with $\epsilon > 0$ but arbitrary small, and let the discontinuous finite element space be given by

$$\mathcal{V}_h := \{v \in L^2(\Omega) : v \circ F_K|_K \in \mathcal{P}_r(\hat{K}), \hat{K} \in \mathcal{K}\}, \quad (2.10)$$

where $F_K : \hat{K} \rightarrow K$ is the respective elemental map for $K \in \mathcal{K}$.

The discontinuous Galerkin method then reads: find $u_h \in \mathcal{V}_h$ such that

$$a(u_h, v) = l(v), \quad \forall v \in \mathcal{V}_h, \quad (2.11)$$

where the bilinear form $a(\cdot, \cdot) : \mathcal{V} \times \mathcal{V} \rightarrow \mathbb{R}$ and the linear form $l(\cdot) : \mathcal{V} \rightarrow \mathbb{R}$ are given by

$$a(v, z) := \sum_{K \in \mathcal{K}} (\alpha \nabla v, \nabla z)_{L^2(K)} - \sum_{e \in \Gamma^I} \left((n \cdot \{\alpha \Pi \nabla v\}_w, [z])_{L^2(e)} \right. \quad (2.12)$$

$$\left. + (n \cdot \{\alpha \Pi \nabla z\}_w, [v])_{L^2(e)} - \frac{\sigma_e \gamma_e}{h_e} ([v], [z])_{L^2(e)} \right),$$

$$l(v) := (f, v)_{L^2(\Omega)}, \quad (2.13)$$

respectively; here $\Pi : (L^2(\Omega))^d \rightarrow (\mathcal{V}_h)^d$ denotes the orthogonal L^2 -projection operator onto $(\mathcal{V}_h)^d$, $h_e := \text{diam}(e)$, and $\sigma_e \in \mathbb{R}$ is a positive constant large enough to make the bilinear form (2.13) coercive with respect to the natural energy norm; we refer, e.g., to [15, 6] and references therein for details on the analysis of DG methods for elliptic problems. Discontinuous Galerkin methods with weighted averages were introduced in [11, 19].

REMARK 2.1. For all $v \in \mathcal{V}_h$, we have $\Pi \nabla v = \nabla v$, therefore the bilinear form (2.12) with $v, z \in \mathcal{V}_h$ is reduced to the more familiar form

$$a(v, z) = \sum_{K \in \mathcal{K}} (\alpha \nabla v, \nabla z)_{L^2(K)} - \sum_{e \in \Gamma^I} \left((n \cdot \{\alpha \nabla v\}_w, [z])_{L^2(e)} \right. \quad (2.14)$$

$$\left. + (n \cdot \{\alpha \nabla z\}_w, [v])_{L^2(e)} - \frac{\sigma_e \gamma_e}{h_e} ([v], [z])_{L^2(e)} \right).$$

3. Multiscale method. In the VMS framework, the finite element solution space \mathcal{V}_h is decoupled into coarse and fine scale contributions, viz., $\mathcal{V}_h = \mathcal{V}_c \oplus \mathcal{V}_f$, with $\mathcal{V}_c \subset \mathcal{V}_h$. The split between the coarse and the fine scales can be determined via an inclusion operator $\mathcal{I}_c : \mathcal{V}_h \rightarrow \mathcal{V}_c$; then, $\mathcal{V}_c := \mathcal{I}_c \mathcal{V}_h$ and $\mathcal{V}_f := (I - \mathcal{I}_c) \mathcal{V}_h = \{v \in \mathcal{V}_h : \mathcal{I}_c v = 0\}$. A particular choice of \mathcal{I}_c will be discussed below.

The multiscale map $\mathcal{T} : \mathcal{V}_c \rightarrow \mathcal{V}_f$ from the coarse to the fine scale is defined as

$$a(\mathcal{T}v_c, v_f) = -a(v_c, v_f) \quad \forall v_c \in \mathcal{V}_c \text{ and } \forall v_f \in \mathcal{V}_f. \quad (3.1)$$

The next step is to decompose u_h and v in (2.11) into coarse and fine scale components. In particular, we have

$$u_h = u_c + \mathcal{T}u_c + u_f \quad (3.2)$$

and $v = v_c + v_f$, with $u_c, v_c \in \mathcal{V}_c$ and $(\mathcal{T}u_c + u_f), v_f \in \mathcal{V}_f$. Then (2.11) is equivalent to the problem: find $u_c \in \mathcal{V}_c$ and $v_f \in \mathcal{V}_f$ such that

$$a(u_c + \mathcal{T}u_c + u_f, v_c + v_f) = l(v_c + v_f), \quad \forall v_c \in \mathcal{V}_c \text{ and } \forall v_f \in \mathcal{V}_f. \quad (3.3)$$

The fine scale component u_f can be computed by letting $v_c = 0$ in (3.3) and using the multiscale map (3.1). We then arrive to the problem: find $u_f \in \mathcal{V}_f$ such that

$$a(u_f, v_f) = l(v_f), \quad \forall v_f \in \mathcal{V}_f. \quad (3.4)$$

The coarse scale solution is obtained by letting $v_f = 0$ in (3.3): find $u_c \in \mathcal{V}_c$ such that

$$a(u_c + \mathcal{T}u_c, v_c) = l(v_c) - a(u_f, v_c), \quad \forall v_c \in \mathcal{V}_c. \quad (3.5)$$

In (3.5), $\mathcal{T}v_c$ and u_f are unknown and obtained by solving (3.1) and (3.4). Note that the linear system (3.5) has $\dim(\mathcal{V}_c)$ unknowns.

3.1. Localization and Discretization. The bilinear form is characterized by more local behaviour in \mathcal{V}_f than in \mathcal{V}_h [30, 31] (at least in the case of conforming AVMS). This motivates us to solve the fine scale equations on (localized) overlapping patches, instead of on the whole domain Ω . The patches are chosen large enough to ensure sufficiently accurate computations of $\mathcal{T}v_c$ and u_f . The computations of the fine scale components of the solution can be done in parallel with localized right hand sides.

To define the coarse space \mathcal{V}_c , we begin by fixing a coarse mesh \mathcal{K}_c . Then, \mathcal{V}_c is defined as the space of discontinuous piecewise linear functions on \mathcal{K}_c , viz.,

$$\mathcal{V}_c := \{v \in L^2(\Omega) : v \circ F_K|_K \in \mathcal{P}_r(\hat{K}), \hat{K} \in \mathcal{K}_c\}. \quad (3.6)$$

DEFINITION 3.1. Let $\{\phi_j : j = 1, \dots, \dim(\mathcal{V}_c)\}$ be the Lagrange basis of \mathcal{V}_c . Let also \mathcal{M}_i to be the set of indices j such that $\phi_j = 1$ on node i , the sum $\Phi_i := \sum_{j \in \mathcal{M}_i} \phi_j$ constructs a standard continuous Lagrangian basis function. We say that ω_i^1 is an 1-layer patch, if $\omega_i^1 = \text{supp}(\Phi_i)$. Further, we say that ω_i^L is an L -layer patch if

$$\omega_i^L = \cup_{\{i: \text{supp}(\Phi_i) \cap \omega_i^{L-1}\} \neq \emptyset} \text{supp}(\Phi_i), \quad L = 2, 3, \dots \quad (3.7)$$

Finally, the set $\omega_i^L \setminus \omega_i^{L-1}$ will be referred to as an L -ring. This is illustrated in Figure 3.1. On each L -layer patch, we introduce the fine mesh $\mathcal{K}_f(\omega_i^L)$ such that $\cup_{K \in \mathcal{K}_f(\omega_i^L)} K = \omega_i^L$. Moreover, we assume that $\mathcal{K}_c|_{\omega_i^L}$ and $\mathcal{K}_f(\omega_i^L)$ are nested, that is, (the closure of) every coarse element $K_c \in \mathcal{K}_c$ coincides with a union of (closures of) fine elements $K_f \in \mathcal{K}_f(\omega_i^L)$. Also, the fine test spaces $\mathcal{V}_f(\omega_i^L)$, corresponding to $\mathcal{K}_f(\omega_i^L)$, are defined by

$$\mathcal{V}_f(\omega_i^L) := \mathcal{V}_f \cap \{v \in L^2(\omega_i^L) : v \circ F_K|_K \in \mathcal{P}_r(\hat{K}), \hat{K} \in \mathcal{K}_f(\omega_i^L)\}. \quad (3.8)$$

Define Γ_i^I to be the union of all interior edges on ω_i^L and Γ_i^B to be the union of all boundary edges on $\partial\omega_i^L$. The bilinear form and localized right hand side used on the patches are then given by

$$\begin{aligned} a_i(v, z) := & \sum_{K \in \mathcal{K}_f(\omega_i^L)} (\alpha \nabla v, \nabla z)_{L^2(K)} - \sum_{e \in \Gamma^I(\omega_i^L)} \left((n \cdot \{\alpha \Pi \nabla v\}_w, [z])_{L^2(e)} \right. \\ & \left. + (n \cdot \{\alpha \Pi \nabla z\}_w, [v])_{L^2(e)} - \frac{\sigma_e \gamma_e}{h_e} ([v], [z])_{L^2(e)} \right), \end{aligned} \quad (3.9)$$

$$l_i(v) := (\Phi_i f, v)_{L^2(\omega_i^L)}. \quad (3.10)$$

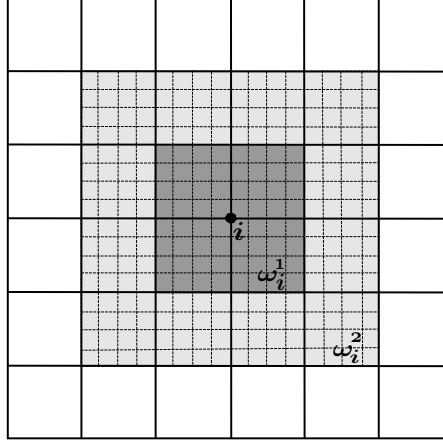


FIGURE 3.1. A patch with one L -ring w_i^1 and two L -rings ω_i^2 around node i in a quadrilateral mesh.

3.2. Discontinuous Galerkin Multiscale method. To fix the fine and coarse scales, we choose the inclusion operator to be the (orthogonal) L^2 -projection \mathcal{P}_c onto the coarse mesh. Denote by \mathcal{N} be the index set of coarse nodes. Each $i \in \mathcal{N}$ corresponds to a patch ω_i^L . For each $i \in \mathcal{N}$ the following local problems need to be solved: find $\tilde{\mathcal{T}}\phi_j \in \mathcal{V}_f(\omega_i^L)$, $\forall j \in \mathcal{M}_i$ and $U_{f,i} \in \mathcal{V}_f(\omega_i^L)$ such that

$$a_i(\tilde{\mathcal{T}}\phi_j, v_f) = -a_i(\phi_j, v_f), \quad \forall v_f \in \mathcal{V}_f(\omega_i^L), \quad (3.11)$$

$$a_i(U_{f,i}, v_f) = l_i(v_f), \quad \forall v_f \in \mathcal{V}_f(\omega_i^L), \quad (3.12)$$

where $a_i(\cdot, \cdot)$ and $l_i(\cdot)$ are defined in (3.9), (3.10). The modified coarse scale problem is formulated as: find $U_c \in \mathcal{V}_c$ such that

$$a(U_c + \tilde{\mathcal{T}}U_c, v_c) = l(v_c) - a(U_f, v_c), \quad \forall v_c \in \mathcal{V}_c. \quad (3.13)$$

Upon setting $U_f := \sum_{i \in \mathcal{N}} U_{f,i}$, the approximate solution to the multiscale problem is given by

$$U = U_c + \tilde{\mathcal{T}}U_c + U_f. \quad (3.14)$$

The above procedure will be referred to as the *discontinuous Galerkin multiscale method*.

We note that the approximation U is *not* equal to u_h in general, since the domain of the fine scale problems is truncated. However, as discussed above it is expected that U is a good approximation to u_h due to the decaying nature of the fine scale solutions away from the respective patch.

3.3. Local conservation property. The DG methods are known to have good local conservation properties in that the normal fluxes are conservative. The ADG-MS inherits this property on the coarse scale. To see this, we introduce the normal fluxes on element $K_c \in \mathcal{K}_c$ by

$$\hat{\sigma}(U) := \begin{cases} \{n \cdot \alpha \nabla U\}_w - \sigma_e \gamma_e h_e^{-1}[U] & e \in \partial K_c \setminus \Gamma^B, \\ 0 & e \in \partial K_c \cap \Gamma^B. \end{cases} \quad (3.15)$$

where $U = U_c + \tilde{T}U_c + U_f$, and each interface e is a face of a fine scale element $K \in \mathcal{K}$, i.e., the number of edges can exceed the number of faces for each element K_c . By setting $w \in \mathcal{V}_c$ to be equal to 1 on the element K_c and 0 otherwise in (2.12), (2.13) and by using the discrete normal fluxes defined in (3.15), we arrive to the discrete element-wise conservation law

$$(f, 1)_{L^2(K_c)} + (\hat{\sigma}(U), 1)_{L^2(\partial K_c)} = 0, \quad (3.16)$$

for all $K_c \in \mathcal{K}_c$.

4. A Posteriori Error Estimate in Energy Norm.

4.1. A posteriori estimate. We shall use the symbol ' \lesssim ' instead of ' $\leq c$ ', when the constant c is independent of H , h and L .

The following approximation results will be used frequently throughout this section. Let π be the orthogonal L^2 -projection operator onto element-wise constant functions. Then π satisfies the following approximation properties: for an element K , we have

$$\|v - \pi v\|_{L^2(K)} \lesssim \frac{h_K}{\sqrt{\alpha_0}} \|\sqrt{\alpha} \nabla v\|_{L^2(K)}, \quad \forall v \in H^1(K), \quad (4.1)$$

$$\|v - \pi v\|_{L^2(\partial K)} \lesssim \sqrt{\frac{h_K}{\alpha_0}} \|\sqrt{\alpha} \nabla v\|_{L^2(K)} \quad \forall v \in H^1(K). \quad (4.2)$$

LEMMA 4.1. *Let $\mathcal{I}_{Os} : \mathcal{V}_h \rightarrow \mathcal{V}_h \cap H^1(\Omega)$ be the Oswald interpolation operator defined as*

$$\mathcal{I}_{Os} v_h = \sum_{i \in \mathcal{N}} \left(\frac{1}{|\mathcal{M}_i|} \sum_{j \in \mathcal{M}_i} v_{h,j}(x_i) \varphi_j \right), \quad (4.3)$$

where φ_j is a DG basis function from \mathcal{V}_h . Then,

$$\|v_h - \mathcal{I}_{Os} v_h\|_{L^2(K)}^2 \lesssim \|\sqrt{h_e} [v_h]\|_{L^2(\partial K \setminus \Gamma^B)}^2, \quad (4.4)$$

$$\|\sqrt{\alpha} \nabla (v_h - \mathcal{I}_{Os} v_h)\|_{L^2(K)}^2 \lesssim \alpha^0 \left\| \frac{1}{\sqrt{h_e}} [v_h] \right\|_{L^2(\partial K \setminus \Gamma^B)}^2. \quad (4.5)$$

hold for all $v_h \in \mathcal{V}_h$ and $K \in \mathcal{K}$. The proof, omitted here, follows closely that of [25]. Lemma 4.1 can also be extended to irregular meshes. There a hierarchical refinement of the mesh is performed to eliminate the hanging nodes; we refer to [26] for details. For irregular meshes the constant in the bounds of Lemma 4.1 also depends on the number of hanging nodes on each face.

REMARK 4.2. *The result in Lemma 4.1 can be sharpened if a locally quasi-monotone [32] distribution of the diffusion tensor is assumed to hold. Then $\alpha^0|_K$ can be replaced by the harmonic mean value γ_e on face e ; see [12].*

THEOREM 4.3. *Let u , u_h be given by (2.1)-(2.2) and (2.11), respectively. Let also $\chi \in \mathcal{V}_h \cap H^1(\Omega)$. Moreover, let $\mathcal{E} := \mathcal{E}_c + \mathcal{E}_d$ where $\mathcal{E}_c := u - \chi$ and $\mathcal{E}_d := \chi - u_h$. Then*

$$\sum_{K \in \mathcal{K}} \|\sqrt{\alpha} \nabla \mathcal{E}_c\|_{L^2(K)}^2 \lesssim \sum_{K \in \mathcal{K}} (\varrho_K(u_h) + \zeta_K(u_h, \chi))^2, \quad (4.6)$$

where

$$\varrho_K(u_h) = \frac{h_K}{\sqrt{\alpha_0}} \|f + \nabla \cdot \alpha \nabla u_h\|_{L^2(K)}, \quad (4.7)$$

$$\begin{aligned} & + \sqrt{\frac{h_K}{\alpha_0}} \left(\|(1 - w_{K(e)})n \cdot [\alpha \nabla u_h]\|_{L^2(\partial K)} + \left\| \frac{\sigma_e \gamma_e}{h_e} [u_h] \right\|_{L^2(\partial K \setminus \Gamma^B)} \right), \\ \zeta_K(u_h, \chi) & = \|\sqrt{\alpha} \nabla(u_h - \chi)\|_{L^2(K)}. \end{aligned} \quad (4.8)$$

Proof. Let π be the L^2 -orthogonal projection onto the element-wise constant functions and define $\eta := \mathcal{E}_c - \pi \mathcal{E}_c$. We then have

$$a(\mathcal{E}, \mathcal{E}_c) = a(u, \mathcal{E}_c) - a(u_h, \mathcal{E}_c) = l(\mathcal{E}_c) - a(u_h, \mathcal{E}_c) = l(\eta) - a(u_h, \eta), \quad (4.9)$$

which implies

$$\sum_{K \in \mathcal{K}} \|\sqrt{\alpha} \mathcal{E}_c\|^2 = a(\mathcal{E}_c, \mathcal{E}_c) = (l(\eta) - a(u_h, \eta)) - a(\mathcal{E}_d, \mathcal{E}_c). \quad (4.10)$$

Upon integration by parts and using the identity $[vw] = \{v\}_w[w] + \{w\}_{\bar{w}}[v]$ where \bar{w} is the skew-weighted average given by

$$\{v\}_{\bar{w}} := w_{K^-(e)}v^+ + w_{K^+(e)}v^-, \quad (4.11)$$

then the first term on the right-hand side of (4.10) yields

$$\begin{aligned} & l(\eta) - a(u_h, \eta) \\ & = \sum_{K \in \mathcal{K}} (f + \nabla \cdot \alpha \nabla u_h, \eta)_{L^2(K)} + \sum_{e \in \Gamma^I} \left(- (n \cdot [\alpha \nabla u_h], \{\eta\}_{\bar{w}})_{L^2(e)} \right. \\ & \quad \left. + (n \cdot \{\alpha \Pi \nabla \eta\}_w, [u_h])_{L^2(e)} - \sigma \gamma_e h_e^{-1} ([u_h], [\eta])_{L^2(e)} \right) \\ & \quad + \sum_{e \in \Gamma^B} (n \cdot \alpha \nabla u_h, \eta)_{L^2(e)}. \end{aligned} \quad (4.12)$$

The first term on the right-hand side of (4.12) and can be bounded as follows,

$$\sum_{K \in \mathcal{K}} (f + \nabla \cdot \alpha \nabla u_h, \eta)_{L^2(\Omega)} \lesssim \sum_{K \in \mathcal{K}} \frac{h_K}{\sqrt{\alpha_0}} \|f + \nabla \cdot \alpha \nabla u_h\|_{L^2(\Omega)} \|\sqrt{\alpha} \nabla \mathcal{E}_c\|_{L^2(\Omega)},$$

using (4.1). The second term on the right-hand side of (4.12) gives

$$\begin{aligned} & \sum_{e \in \Gamma^I} (n \cdot [\alpha \nabla u_h], \{\eta\}_{\bar{w}})_{L^2(e)} \\ & \lesssim \sum_{K \in \mathcal{K}} \sqrt{\frac{h_K}{\alpha_0}} \|(1 - w_{K(e)})n \cdot [\alpha \nabla u_h]\|_{L^2(\partial K \setminus \Gamma^B)} \|\sqrt{\alpha} \nabla \mathcal{E}_c\|_{L^2(K)}, \end{aligned} \quad (4.13)$$

using (4.2). For the third term on the right-hand side of (4.12), noting that $\nabla \eta = \nabla \mathcal{E}_c$, we deduce

$$\sum_{e \in \Gamma^I} (n \cdot \{\alpha \Pi \nabla \mathcal{E}_c\}_w, [\mathcal{E}_d])_{L^2(e)} \lesssim \sum_{K \in \mathcal{K}} \frac{1}{\sqrt{h_K \alpha_0}} \|\gamma_e [\mathcal{E}_d]\|_{L^2(\partial K \setminus \Gamma^B)} \|\sqrt{\alpha} \nabla \mathcal{E}_c\|_{L^2(K)},$$

using an inverse estimate and the L^2 -stability of Π . For the last term on the right-hand side of (4.12), we have

$$\sum_{e \in \Gamma^I} \frac{\sigma_e \gamma_e}{h_e} ([u_h], [\eta])_{L^2(e)} \lesssim \sum_{K \in \mathcal{K}} \sqrt{\frac{h_K}{\alpha_0}} \left\| \frac{\sigma_e \gamma_e}{h_e} [u_h] \right\|_{L^2(\partial K \setminus \Gamma^B)} \|\sqrt{\alpha} \nabla \mathcal{E}_c\|_{L^2(K)}.$$

The last term on the right-hand side of (4.10),

$$a(\mathcal{E}_d, \mathcal{E}_c) = \sum_{K \in \mathcal{K}} (\alpha \nabla \mathcal{E}_d, \nabla \mathcal{E}_c)_{L^2(K)} - \sum_{e \in \Gamma^I} (\{\alpha \Pi \nabla \mathcal{E}_c\}_w, [\mathcal{E}_d]), \quad (4.14)$$

can be bounded as follows: the first term in (4.14), yields

$$\sum_{K \in \mathcal{K}} (\alpha \nabla \mathcal{E}_d, \nabla \mathcal{E}_c)_{L^2(K)} \lesssim \sum_{K \in \mathcal{K}} \|\sqrt{\alpha} \nabla \mathcal{E}_d\|_{L^2(K)} \|\sqrt{\alpha} \nabla \mathcal{E}_c\|_{L^2(K)}, \quad (4.15)$$

while the second term has already been treated.

Combining all the above bounds, the result follows. \square

REMARK 4.4. *The bound (4.6) is not an a posteriori bound as χ is not given (although its definition is at our disposal). Setting $\chi = \mathcal{I}_{Os} u_h$, we arrive to an a posteriori bound whereby χ can either be evaluated directly, or estimated using Lemma 4.1. Another possible choice is a weighted Oswald-type interpolation operator with the weights depending on the diffusion tensor [4].*

REMARK 4.5. *Concerning the lower efficiency bounds, the term (4.7) is robust with respect to the diffusion tensor; see [18]. But to prove that (4.8) is robust with respect to the diffusion tensor, to the authors' knowledge, a locally quasi-monotone distribution of the diffusion tensor has to hold. Under this assumption (4.8) can be estimated and hidden by the other terms in (4.7).*

THEOREM 4.6. *Let u, U be defined in (2.1)-(2.2) and (3.14), respectively and set $X = \mathcal{I}_{Os} U \in H^1(\Omega)$. Set $\mathcal{E} := \mathcal{E}_c + \mathcal{E}_d$ where $\mathcal{E}_c := u - X$ and $\mathcal{E}_d := X - U$. Define $U_i := \sum_{j \in \mathcal{M}_i} U_{c,j} (\phi_j + \tilde{T} \phi_j) + U_{f,i}$, where $U_{c,j}$ are the nodal values calculated by (3.13). Then, \mathcal{E}_c satisfies the estimate*

$$\sum_{K \in \mathcal{K}} \|\sqrt{\alpha} \nabla \mathcal{E}_c\|_{L^2(K)}^2 \lesssim \sum_{K_c \in \mathcal{K}_c} \rho_{h,K_c}^2 + \sum_{i \in \mathcal{N}} \rho_{L,\omega_i^L}^2, \quad (4.16)$$

where

$$\rho_{L,\omega_i^L}^2 = \sum_{e \in \Gamma^B(\omega_i^L) \setminus \Gamma^B} \rho_{L,\omega_i^L,e}^2, \quad (4.17)$$

$$\rho_{L,\omega_i^L,e} = \frac{H_{\omega_i^L}}{\sqrt{h_K \alpha_0}} \left(\|n \cdot \{\alpha \nabla U_i\}_w\|_{L^2(e)} + \frac{\sigma_e \gamma_e}{h_e} \| [U_i] \|_{L^2(e)} \right), \quad (4.18)$$

measures the effect of the truncated patches, and

$$\rho_{h,K_c}^2 = \sum_{K \in K_c} (\varrho_K(U) + \zeta_K(U, X))^2, \quad (4.19)$$

with ϱ_K and ζ_K as in Theorem 4.3.

Proof. First, notice that

$$\sum_{K \in \mathcal{K}} \|\sqrt{\alpha} \nabla \mathcal{E}_c\|_{L^2(K)}^2 = a(e_c, e_c) = a(\mathcal{E}, \mathcal{E}_c) - a(\mathcal{E}_d, \mathcal{E}_c). \quad (4.20)$$

Then, using (2.11) and the fine scale equations (3.11)–(3.12), we have

$$a(\mathcal{E}, \mathcal{E}_c) = a(\mathcal{E}, \mathcal{E}_c - v_c), \quad (4.21)$$

$$= l(\mathcal{E}_c - v_c) - a(U, \mathcal{E}_c - v_c), \quad (4.22)$$

$$= \sum_{i \in \mathcal{N}} \left(l_i(\mathcal{E}_c - v_c) - a(U_i, \mathcal{E}_c - v_c) \right), \quad (4.23)$$

$$= \sum_{i \in \mathcal{N}} \left(l_i(\mathcal{E}_c - v_c - v_f) - a(U_i, \mathcal{E}_c - v_c) + a_i(U_i, v_f) \right), \quad (4.24)$$

for any $v_c \in \mathcal{V}_c$ and $v_f \in \mathcal{V}_f(\omega_i^L)$, for all $i \in \mathcal{N}$. From (2.12) and (3.9) we obtain

$$\begin{aligned} a_i(U_i, v_f) &= a(U_i, v_f) + \sum_{e \in \Gamma^B(\omega_i^L) \setminus \Gamma^B} \left((n \cdot \{\alpha \nabla U_i\}_w, [v_f])_{L^2(e)} \right. \\ &\quad \left. + (n \cdot \{\alpha \nabla v_f\}_w, [U_i])_{L^2(e)} - \frac{\sigma_e \gamma_e}{h_e} ([U_i], [v_f])_{L^2(e)} \right). \end{aligned} \quad (4.25)$$

Then, applying (4.25) on (4.24), we deduce

$$\begin{aligned} a(\mathcal{E}, \mathcal{E}_c) &= \left(l(\mathcal{E}_c - v_c - v_f) - a(U, \mathcal{E}_c - v_c - v_f) \right) \\ &\quad + \sum_{i \in \mathcal{N}} \sum_{e \in \Gamma^B(\omega_i^L) \setminus \Gamma^B} \left((n \cdot \{\alpha \nabla U_i\}_w, [v_f])_{L^2(e)} + (n \cdot \{\alpha \nabla v_f\}_w, [U_i])_{L^2(e)} \right. \\ &\quad \left. - \frac{\sigma_e \gamma_e}{h_e} ([U_i], [v_f])_{L^2(e)} \right) \\ &=: I + II. \end{aligned} \quad (4.26)$$

Term I can be estimated as in the proof of Theorem 4.3, upon selecting $v_c := \pi_c \mathcal{E}_c$ and $v_f = \pi_f(\mathcal{E}_c - \pi_c \mathcal{E}_c) = \pi_f \mathcal{E}_c$, where π_c and π_f are the element-wise constant L^2 -orthogonal projections onto the coarse space \mathcal{V}_c on the fine space \mathcal{V}_f , respectively. (We note that, by construction, $\pi_f \pi_c v = 0$, for all $v \in \mathcal{V}_h$.)

Since v_f is chosen to be piecewise constant the second term in II is equal to zero. For each $i \in \mathcal{N}$, and for each $e \in \Gamma^B(\omega_i^L) \setminus \Gamma^B$, we have

$$\begin{aligned} &\left| (n \cdot \{\alpha \nabla U_i\}_w, [v_f])_{L^2(e)} - \frac{\sigma_e \gamma_e}{h_e} ([U_i], [v_f])_{L^2(e)} \right| \\ &\lesssim \rho_{L, \omega_i^L, e} \frac{\sqrt{h_K \alpha_0}}{H_{\omega_i^L}} \|[v_f]\|_{L^2(e)}, \end{aligned} \quad (4.27)$$

using (4.28) and the Cauchy-Schwarz inequality. To bound the term involving v_f , we work as follows:

$$\begin{aligned} \frac{h_K \alpha_0}{H_{\omega_i^L}^2} \|[v_f]\|_{L^2(e)}^2 &\lesssim \sum_{K \in \{K^+, K^-\}} \frac{\alpha_0}{H_{\omega_i^L}^2} \|v_f\|_{L^2(K)}^2 \\ &\lesssim \sum_{K \in \{K^+, K^-\}} \frac{\alpha_0}{H_{\omega_i^L}^2} \|\mathcal{E}_c - \pi_c \mathcal{E}_c\|_{L^2(K)}^2 \lesssim \sum_{K \in \{K^+, K^-\}} \alpha_0 \|\nabla \mathcal{E}_c\|_{L^2(K)}^2 \\ &\lesssim \sum_{K \in \{K^+, K^-\}} \|\sqrt{\alpha} \nabla \mathcal{E}_c\|_{L^2(K)}^2, \end{aligned} \quad (4.28)$$

using a trace inequality, and the L^2 -stability of π_f , viz., $\|\pi_f v\|_{L^2(K)} \leq \|v\|_{L^2(K)}$.

Combining the above and summing over all patches, using the discrete version of the Cauchy-Schwarz inequality, the proof is concluded.

□

5. Implementation and Adaptivity. The system of equations arising from the discretization of the modified coarse multiscale problem (3.13) is given by

$$(A + T)U = b - d, \quad (5.1)$$

where $A_{i,j} = a(\phi_i, \phi_j)$, $T_{i,j} = a(\tilde{\mathcal{T}}\phi_i, \phi_j)$, $b_i = l(\phi_i)$ and $d_i = a(U_f, \phi_i)$, for all $i, j \in \mathcal{N}$. To assemble the right and left hand sides of (5.1), $\tilde{\mathcal{T}}\phi_i$ and $U_{f,i}$ need to be computed for all $i \in \mathcal{N}$. This can be done in parallel since no commutation is needed between the different fine scale problems. For each fine scale problem it is also possible to assemble $A(i, j) = a(\phi_i, \phi_j)$, $T(i, j) = a(\tilde{\mathcal{T}}\phi_i, \phi_j)$, $b_i = l(\phi_i)$ $d_i = \sum_{j \in \mathcal{N}} a(U_{f,j}, \phi_i)$ for a fixed i and for all j such that $\mu_d(\text{supp}(\phi_j) \cap \omega_i) > 0$. The constraints needed on the fine scale test spaces to solve $\tilde{\mathcal{T}}\phi_i$ and $U_{f,i}$ are $\mathcal{V}_f = \{v \in \mathcal{V}^h : \mathcal{P}_c v = 0\}$, which are implemented using Lagrange multipliers. The spaces \mathcal{V}_f and \mathcal{V}_c are orthogonal with respect to the L^2 -inner product.

Let $\mathcal{V}_c = \text{span}\{\phi_i\}$ and $\mathcal{V}_f = \text{span}\{\varphi_i\}$. Then, the system of equations to be solved on the fine scale is given by

$$\begin{pmatrix} K & P^T \\ P & 0 \end{pmatrix} \xi = \begin{pmatrix} b \\ 0 \end{pmatrix}, \quad (5.2)$$

where

$$P = \begin{pmatrix} (\phi_1, \varphi_1) & (\phi_1, \varphi_2) & \dots & (\phi_1, \varphi_N) \\ (\phi_2, \varphi_1) & (\phi_2, \varphi_2) & \dots & (\phi_2, \varphi_N) \\ \vdots & \vdots & \ddots & \vdots \\ (\phi_M, \varphi_1) & (\phi_M, \varphi_2) & \dots & (\phi_M, \varphi_N) \end{pmatrix}, \quad (5.3)$$

with $K_{k,l} = a_i(\varphi_k, \varphi_l)$ and b either $b_k = l_i(\varphi_k)$ for (3.12) or $b_k = -a_i(\phi_i, \varphi_k)$ for (3.11).

Using the a posteriori error estimate above it is possible to design an adaptive algorithm that automatically tunes the fine mesh size and the size of the patches. In the numerical experiments below, we have implemented Algorithm 1, which extends the patches in all directions and uses a uniform mesh refinement on each patch. A more elaborate algorithm which only extends in the direction where the error is large and uses adaptive mesh refinement on each patch would be a possible extension, since the a posteriori indicators above contain local contributions of each individual patch-boundary face and of each fine scale element residual.

6. Numerical examples.

6.1. Decay of the fine scale solution. We consider the fine scale problem: find $\tilde{\mathcal{T}}_L \Phi_i \in \mathcal{V}_f(\omega_i^L)$ such that

$$a_i(\tilde{\mathcal{T}}_L \Phi_i, v) = -a_i(\Phi_i, v), \quad \forall v \in \mathcal{V}_f(\omega_i^L), \quad (6.1)$$

for $L = 1, 2, \dots, N$. We have $\omega_i^L \subseteq \Omega := [0, 1]^2$ where equality occurs for $L = N$; then $\tilde{\mathcal{T}}_N = \mathcal{T}$. The coarse mesh \mathcal{K}_c on Ω consists of 8×8 coarse elements where each element $K_c \in \mathcal{K}_c \cap \omega_i^L$ is further subdivided into 8×8 fine scale elements $K_f \in \mathcal{K}_f(\omega_i^L)$. The following permeabilities, *One*, *Period* and *SPE31*¹, have been used for the numerical example; the permeabilities are shown in Figure 6.1. In *One*, we have $\alpha = 1$, in

¹Data is taken from the tenth SPE comparative solution project <http://www.spe.org/web/csp/>

Algorithm 1 Adaptive Discontinuous Galerkin Multiscale Method

```

1: Initialize the coarse mesh with mesh size  $H$ .
2: Let the fine mesh size be  $h_K = H/2$  for all  $K_c \in \mathcal{K}_c$  and  $L(\omega_i) = 2$  for all  $i \in \mathcal{N}$ .
3: while  $\sum_{i \in \mathcal{N}} (\rho_{h, \omega_i}^2 + \rho_{L, \omega_i}^2) > TOL$  do
4:   for  $i \in \mathcal{N}$  do
5:     Solve the fine scale problems (3.1) and (3.12).
6:     Compute the matrix and vector entries on the coarse scale.
7:   end for
8:   Solve the modified coarse scale problem (3.13) .
9:   for  $i \in \mathcal{N}$  do
10:    if  $\rho_{L, \omega_i}^2 > TOL/(2N)$  then
11:       $L(\omega_i) := L(\omega_i) + 1$ 
12:    end if
13:  end for
14:  for  $K_c \in \mathcal{K}_c$  do
15:    if  $\rho_{h, K}^2 > TOL/(2|\mathcal{K}_c|)$  then
16:       $h_K := h_K/2$ 
17:    end if
18:  end for
19: end while

```

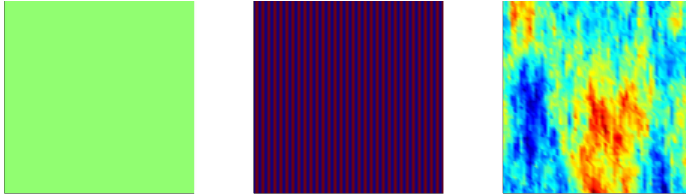


FIGURE 6.1. Permeability structure of One, Period and SPE31 in log scale.

Period $\alpha = 1$ or $\alpha = 0.1$ with a period of $1/64$ in the x -direction, and in *SPE31* the data is taken from the SPE comparative solution project and projected into a 64×64 domain, see Figure 6.1. The error is measured in the relative broken energy norm

$$E(\tilde{\mathcal{T}}_L \Phi_i, \mathcal{T} \Phi_i) = \frac{(\sum_{K \in \mathcal{K}_f(\omega_i^N)} \|\sqrt{\alpha} \nabla (\tilde{\mathcal{T}}_L \Phi_i - \mathcal{T} \Phi_i)\|^2)^{1/2}}{(\sum_{K \in \mathcal{K}_f(\omega_i^N)} \|\sqrt{\alpha} \nabla \mathcal{T} \Phi_i\|^2)^{1/2}}, \quad (6.2)$$

where $\tilde{\mathcal{T}}_L \Phi_i$ is the solution to (6.1) on patch ω_i^L and $\mathcal{T} \Phi_i$ is the solution to (6.1) on patch $\omega_i^N = \Omega$.

Exponential decay is observed with respect to the number of L -rings in the relative energy norm, see Figure 6.2. This is in accordance with the recent result for the conforming method in [30, 31]. The solutions to (6.1) using the different permeabilities for $L = 2$ are illustrated in Figure 6.3. We observed that, due to the fast decay of the localized fine scale contributions, it is sufficient to solve the fine scale problem on a patch $\omega_i^L \subset \Omega$ using a small number of L -rings, without any significant compromise to the quality of the approximate solution. Evidently, this, in turn, means significant savings in terms of computational work.

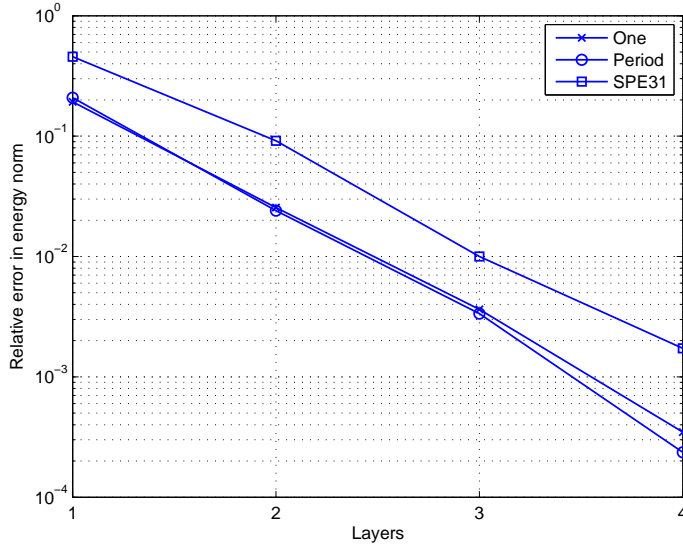


FIGURE 6.2. Convergence of $E(\tilde{\mathcal{T}}_L \Phi_i, \mathcal{T} \Phi_i)$ when $L = 1, \dots, 4$ in equation (6.1) for the different permeabilities.

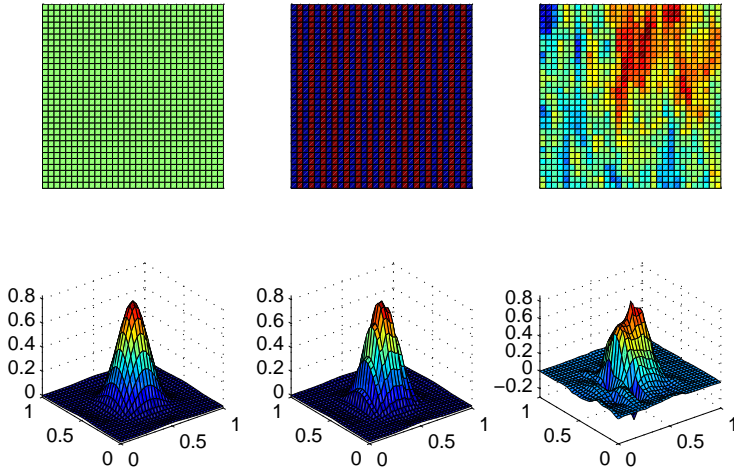


FIGURE 6.3. The solution $\tilde{\mathcal{T}}_L \Phi_i$ to (6.1) using $L = 2$ for permeabilities One (left), Period (center) and SPE31 (right). The projected permeability is illustrated above for each corresponding solution.

6.2. Convergence. We consider the model problem (2.1)–(2.2) on the unit square $\Omega = [0, 1]^2$, with forcing function $f = -1$ in the lower left corner $\{0 \leq x, y \leq 1/64\}$, $f = 1$ in the upper right corner $\{63/64 \leq x, y \leq 1\}$, and $f = 0$ otherwise. The same permeabilities as in Section 6.1 are used. The computational domain Ω is again split into 8×8 coarse square elements, where each coarse element $K \in \mathcal{K}_c$

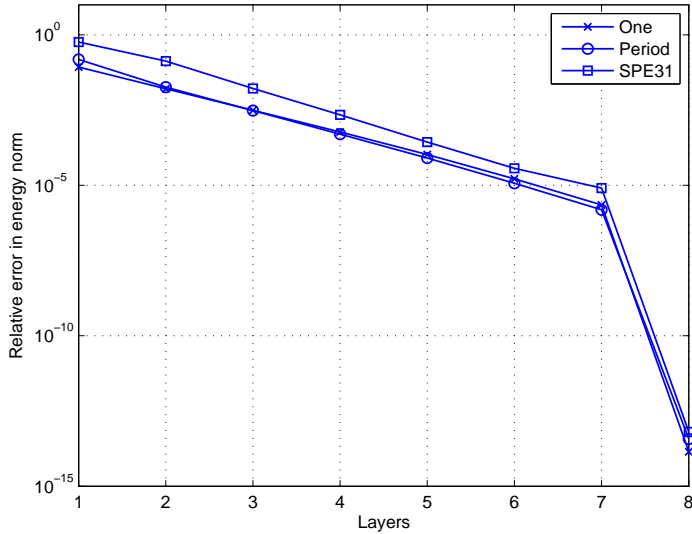


FIGURE 6.4. Convergence in relative energy norm $E(U_L, u_h)$, equation (2.1)-(2.2), when L increases using the different permeabilities One, Period and SPE31.

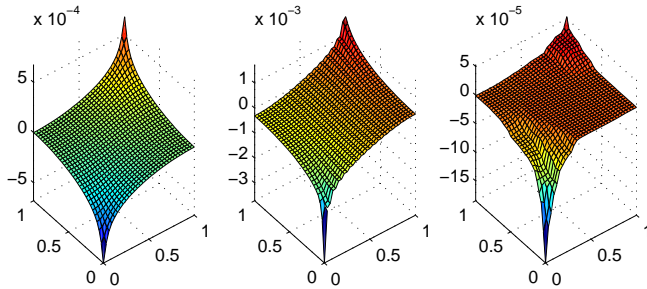


FIGURE 6.5. Reference solution to One, Period and SPE31.

is further subdivided into 8×8 fine square elements. The error is measured in the relative broken energy norm

$$E(U_L, u_h) = \frac{(\sum_{K \in \mathcal{K}} \|\sqrt{\alpha} \nabla(U_L - u_h)\|^2)^{1/2}}{(\sum_{K \in \mathcal{K}} \|\sqrt{\alpha} \nabla u_h\|^2)^{1/2}}, \quad (6.3)$$

where u_h is the DG solution computed on 64×64 elements. Exponential decay is observed with respect to the number of L -rings for the different permeabilities *One*, *Period* and *SPE31*, until the patches covers the whole domain when $L = 8$; this is illustrated in Figure 6.4. As expected, when $L = 8$, only round off error between the multiscale solution and the reference solution is observed.

6.3. Adaptivity. We consider the problem (2.1)–(2.2) on the unit square $\Omega = [0, 1]^2$, with forcing function $f = -1$ in the lower left corner $\{0 \leq x, y \leq 1/128\}$, $f = 1$ in the upper right corner $\{127/128 \leq x, y \leq 1\}$, and $f = 0$ otherwise. The following permeabilities *SPE11*, *SPE21*, *SPE31* and *SPE41* are used and projected

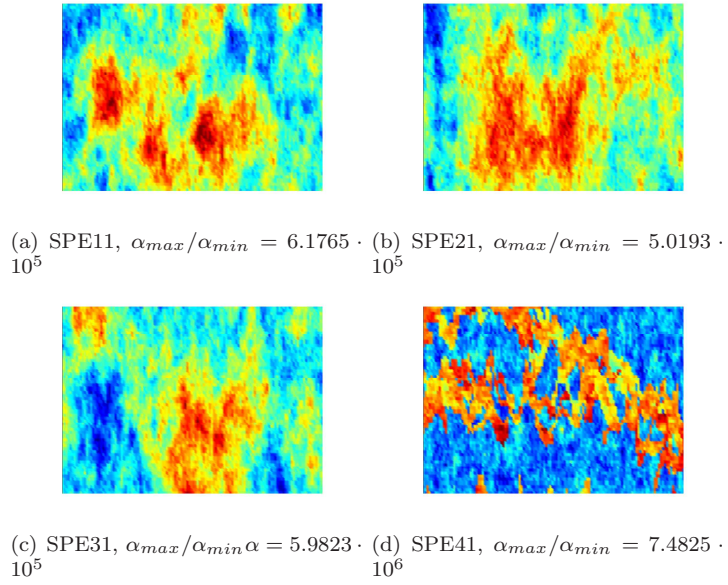


FIGURE 6.6. Permeabilities projection in log scale.

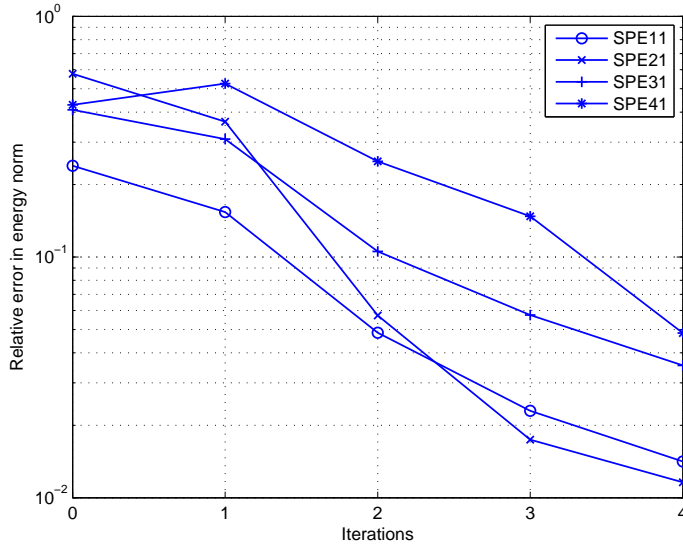
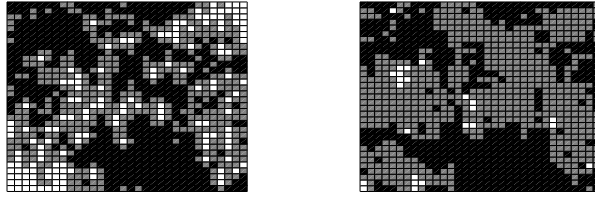


FIGURE 6.7. Relative in error broken energy norm against the number of iterations.

into a 128×128 domain, see Figure 6.6. The computational domain Ω is split into 32×32 coarse square elements $K_c \in \mathcal{K}_c$. The error is measured in the relative energy norm $E(\cdot)$, defined in (6.3), with the reference solution u_h being the DG solution computed on a 256×256 -element mesh.

Algorithm 1 are performed, with a modification in the marking strategy. We refine the fine scale mesh in 30% of the coarse elements and increase the patch size



(a) Levels of fine mesh refinements: one refinement (black), two refinements (grey), three refinements (white) (b) Patch sizes L used: $L = 2$ (black), $L = 3$ (grey), $L = 4$ (white).

FIGURE 6.8. *Refinement levels and patch sizes for SPE41.*

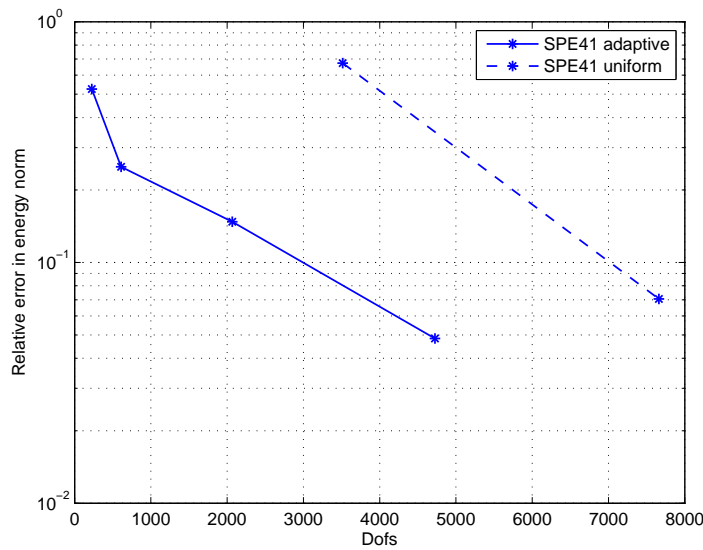


FIGURE 6.9. *The relative error with respect to the mean value of the degrees of freedom for the fine scale problems.*

for 30% of the local problems. In Iteration 0, the standard DG solution on the coarse mesh is used. In Iteration 1 the multiscale problem is solved using one refinement on each coarse element and each fine scale problem is solved with $L = 2$, and so on. Even though complicated permeabilities with $\alpha_{max}/\alpha_{min} \sim 10^6$ are used, the proposed adaptive algorithm is able to reduce relative error is to less than 5% in all cases; this is shown in Figure 6.7. Using Algorithm 1, most computational work is put in the areas around the injector ($f = -1$ in lower left corner), the producer ($f = 1$ in the upper right corner), and in the high permeability areas in Ω , see Figure 6.6. For the case of *SPE41*, this is illustrated in Figure 6.8: (a) shows the levels of refinement of the fine mesh in each coarse scale elements, and (b) shows the respective patch sizes L used. The black fields correspond to the initial value, the grey fields stand for initial value +1, and the white fields stand for initial value +2. The initial values are, (a) one refinement and, (b) patch size $L=2$.

The computational work needed to get the same accuracy using Algorithm 1 compared to using uniform refinement on the patch sizes, where the refinement level is kept at the reference level, is illustrated in Figure 6.9. The error in the relative broken energy norm is related to the mean values of the degrees of freedom for the fine scale problems. It is evident that, using the adaptive algorithm, the number of degrees of freedom is reduced considerably compared to uniform refinement, even for the complicated crack shaped permeability *SPE41*, where $\alpha_{max}/\alpha_{min} \sim 10^6$.

7. Concluding remarks. An adaptive multiscale method based on discontinuous Galerkin discretization has been proposed and assessed in practice. Due to the good local conservation of the state variable property it admits, the new method appears to perform very well when applied to challenging standard benchmark problems.

The adaptive algorithm, based on an energy norm a posteriori bound, is shown to lead to substantial computational savings when applied to porous media flow applications, compared to the same method applied on uniform meshes. The multiscale method and the adaptive algorithm admit naturally parallel implementation, which is expected to result in further savings in computational time.

REFERENCES

- [1] J. Aarnes and B.-O. Heimsund, *Multiscale discontinuous Galerkin methods for elliptic problems with multiple scales*, Lecture Notes in Computational Science and Engineering, vol. 44, Springer Berlin Heidelberg, 2005.
- [2] A. Abdulle, *Discontinuous Galerkin finite element heterogeneous multiscale method for elliptic problems with multiple scales*, To appear <http://dx.doi.org/10.1090/S0025-5718-2011-02527-5>, 2011.
- [3] R. A. Adams, *Sobolev spaces*, Academic Press, New York, 1975.
- [4] M. Ainsworth, *Robust a posteriori error estimation for nonconforming finite element approximation*, SIAM Journal on Numerical Analysis **42** (2005), no. 6, pp. 2320–2341.
- [5] D. N. Arnold, *An interior penalty finite element method with discontinuous elements*, SIAM J. Numer. Anal. **19** (1982), no. 4, 742–760. MR 664882 (83f:65173)
- [6] D. N. Arnold, F. Brezzi, B. Cockburn, and L. Marini, *Unified analysis of discontinuous Galerkin methods for elliptic problems*, SIAM J. Numer. Anal. **39** (2001), no. 5, 1749–1779.
- [7] I. Babuška, G. Caloz, and J. E. Osborn, *Special finite element methods for a class of second order elliptic problems with rough coefficients*, SIAM J. Numer. Anal. **31** (1994), no. 4, 945–981.
- [8] I. Babuška and J. E. Osborn, *Generalized finite element methods: their performance and their relation to mixed methods*, SIAM J. Numer. Anal. **20** (1983), no. 3, 510–536.
- [9] G. A. Baker, *Finite element methods for elliptic equations using nonconforming elements*, Math. Comp. **31** (1977), no. 137, 45–59.
- [10] S. C. Brenner and L. R. Scott, *The mathematical theory of finite element methods*, Springer Verlag, 1979.
- [11] E. Burman and P. Zunino, *A domain decomposition method based on weighted interior penalties for advection-diffusion-reaction problems*, SIAM J. Numer. Anal. **44** (2006), no. 4, 1612–1638 (electronic). MR 2257119 (2007m:65123)
- [12] Z. Cai, X. Ye, and S. Zhang, *Discontinuous galerkin finite element methods for interface problems: A priori and a posteriori error estimations*, SIAM Journal on Numerical Analysis **49** (2011), no. 5, 1761–1787.
- [13] J. Chu, Y. Efendiev, V. Ginting, and T. Y. Hou, *Flow based oversampling technique for multiscale finite element methods*, Advances in Water Resources **31** (2008), no. 4, 599–608.
- [14] B. Cockburn, G. E. Karniadakis, and C-W. Shu (eds.), *Discontinuous Galerkin methods*, Lecture Notes in Computational Science and Engineering, vol. 11, Springer-Verlag, Berlin, 2000, Theory, computation and applications, Papers from the 1st International Symposium held in Newport, RI, May 24–26, 1999.
- [15] D. A. Di Pietro and A. Ern, *Mathematical aspects of discontinuous galerkin methods*, Mathématiques et Applications, vol. 69, Springer, 2012.
- [16] W. E, *Principles of multiscale modeling*, Mathematical Modeling and Methods, Cambridge University Press, 2011.

- [17] Y. Efendiev and T. Y. Hou, *Multiscale finite element methods*, Surveys and Tutorials in the Applied Mathematical Sciences, vol. 4, Springer, New York, 2009, Theory and applications.
- [18] A. Ern and A.F. Stephansen, *A posteriori energy-norm error estimates for advection-diffusion equations approximated by weighted interior penalty methods*, J. Comput. Math. **26** (2008), no. 4, 488–510.
- [19] A. Ern, A.F. Stephansen, and P. Zunino, *A discontinuous Galerkin method with weighted averages for advection-diffusion equations with locally small and anisotropic diffusivity*, IMA Journal of Numerical Analysis **29** (2009), no. 2, 235–256.
- [20] J. S. Hesthaven and T. Warburton, *Nodal discontinuous Galerkin methods*, Texts in Applied Mathematics, vol. 54, Springer, New York, 2008, Algorithms, analysis, and applications.
- [21] T. Y. Hou, T. Y. Hou, and X.-H. Wu, *A multiscale finite element method for elliptic problems in composite materials and porous media*, Journal of Computational Physics **134** (1997), 169–189.
- [22] T. Hughes, *Multiscale phenomena: Green’s functions, the Dirichlet-to-Neumann formulation, subgrid scale models, bubbles and the origins of stabilized methods*, Computer Methods in Applied Mechanics and Engineering **127** (1995), no. 1-4, 387–401.
- [23] T. Hughes, G. Feijóo, L. Mazzei, and J.-B. Quinicy, *The variational multiscale method—a paradigm for computational mechanics*, Computer Methods in Applied Mechanics and Engineering **166** (1998), no. 1-2, 3 – 24.
- [24] C. Johnson and J. Pitkäranta, *An analysis of the discontinuous Galerkin method for a scalar hyperbolic equation*, Math. Comp. **46** (1986), no. 173, 1–26.
- [25] O. Karakashian and F. Pascal, *A posteriori error estimates for a discontinuous Galerkin approximation of second-order elliptic problems*, SIAM J. Numer. Anal. **41** (2003), 2374–2399.
- [26] O. Karakashian and F. Pascal, *Adaptive discontinuous Galerkin approximation of second-order elliptic problems*, In Proceedings of the European Congress on Computational Methods in Applied Sciences and Engineering ECCOMAS 2004. P. Neittaanmäki et al. eds. Jyväskylä, 24-28 July 2004.
- [27] M. G. Larson and A. Målqvist, *Adaptive variational multiscale methods based on a posteriori error estimation: Energy norm estimates for elliptic problems*, Computer Methods in Applied Mechanics and Engineering **196** (2007), no. 21-24, 2313–2324.
- [28] P. Lesaint and P.-A. Raviart, *On a finite element method for solving the neutron transport equation*, Mathematical aspects of finite elements in partial differential equations (Proc. Sympos., Math. Res. Center, Univ. Wisconsin, Madison, Wis., 1974), Math. Res. Center, Univ. of Wisconsin-Madison, Academic Press, New York, 1974, pp. 89–123. Publication No. 33.
- [29] A. Målqvist, *Multiscale methods for elliptic problems*, Multiscale Modeling & Simulation **9** (2011), no. 3, 1064–1086.
- [30] A. Målqvist, *A priori error analysis of a multiscale method*, submitted, 2011.
- [31] A. Målqvist and D. Peterseim, *Localization of elliptic multiscale problems*, submitted, 2011.
- [32] M. Petzoldt, *A posteriori error estimators for elliptic equations with discontinuous coefficients*, Advances in Computational Mathematics **16** (2002), 47–75.
- [33] W. H. Reed and T. R. Hill, *Triangular mesh methods for the neutron transport equation.*, Tech. report, Los Alamos Scientific Laboratory, 1973.
- [34] B. Rivière, *Discontinuous Galerkin methods for solving elliptic and parabolic equations*, Frontiers in Applied Mathematics, vol. 35, Society for Industrial and Applied Mathematics (SIAM), Philadelphia, PA, 2008, Theory and implementation.
- [35] W. Wang, *Multiscale discontinuous Galerkin methods and applications*, ProQuest LLC, Ann Arbor, MI, 2008, Thesis (Ph.D.)—Brown University.
- [36] W. Wang, J. Guzmán, and C.-W. Shu, *The multiscale discontinuous Galerkin method for solving a class of second order elliptic problems with rough coefficients*, Int. J. Numer. Anal. Model. **8** (2011), no. 1, 28–47.
- [37] L. Yuan and C.-W. Shu, *Discontinuous Galerkin method based on non-polynomial approximation spaces*, J. Comput. Phys. **218** (2006), no. 1, 295–323.
- [38] L. Yuan and C.-W. Shu, *Discontinuous Galerkin method for a class of elliptic multi-scale problems*, Internat. J. Numer. Methods Fluids **56** (2008), no. 8, 1017–1032.